NTNU

Norwegian University of
Science and Technology

Study of water self-diffusion in healthy fibroglandular breast tissue

Jacob Prescott

Master of Science in Physics and Mathematics
Submission date: June 2017
Supervisor: Pål Erik Goa, IFY

Norwegian University of Science and Technology
Department of Physics

Awknowledgement

This thesis is the final part of my masters degree at the Norwegian University of Science and Technology. I would like to thank my supervisor, Associate Professor Pål Erik Goa, for providing invaluable guidance along the way this semester. He has been an excellent supervisor providing both insight and motivation. I would like to thank the MRI radiographers at the Gastro Centre at St. Olav for running our MR sequences. A special thank you goes out to the volunteers who took time out of their busy schedules to be subjected to said MR sequences.

Finally, I would like to thank my parents, my sisters and my brother supporting me through these long years at the university.

Jacob Prescott
Trondheim, June 25, 2017

Summary

Magnetic resonance imaging (MRI) is an important imaging modalty available in modern medical diagnostics. Novel MR scanner software made available from the vendor was implemented on a clinical MR-scanner. MR measurements were made on fibro glandular tissue (FGT) *in vivo* from healthy volunteers and and also on prepared solutions of bakers yeast (*S. Cerevisiae*). The apparent diffusion coefficient (ADC) and T_2 values were calculated for both. An attempt was made to explain the signal behaviour in the yeast samples by using biophysical models. Across the range of echo times (TE) explored, ADC varied. In the same manner, across the range of b-values explored, the value of T_2 varied. These results suggest some dependence of ADC on TE and T_2 on b-value. A slight change in ADC was detected when only varying the diffusion time in the experiment. For FGT, the signal behaviour varied between subjects and between left and right breast. Significant eddy current artifacts were present across the images aquired.

Sammendrag

Magnetisk resonansavbildning er en viktig avbildningsmodalitet tilgjengelig i moderne medisinsk diagnostikk. Ny programvare til en MR-maskin ble gjort tilgjengelig av leverandøren og ble implementert. Målinger ble gjort på fibroglandulært vev *in vivo* fra friske frivillige og på preparerte løsninger av bakegjær. ADC- og T_2-verdier ble kalkulert for begge. Et forsøk ble gjort på å forklare signaloppførselsen i gjærprøvene ved å bruke biofysiske modeller. Videre, over de verdier av TE benyttet, så varierte ADC. På samme måte varierte T_2 over de b-verdier som ble benyttet. Disse funnene hinter om en avhengighet av ADC på TE og T_2 på b-verdi. Mindre endringer i ADC ble oppdaget når kun diffusjonstiden ble endret i eksperimentet. For FGT var varierte signaloppførselen mellom frivillige og mellom høyre og venstre bryst. Fremtredende virvelstrømartifakter ble påvist i bildene.

Table of Contents

List of abbreviations and terms

Term		*Definition*
ADC	=	Apparent diffusion coefficient
b	=	Degree of diffusion weighing
B_0	=	Main static magnetic field
B_1	=	Circularly polarized magnetic field (RF pulse)
BP	=	Bipolar diffusion gradient
DWI	=	Diffusion weighted imaging
EPI	=	Echo planar imaging
f	=	Fast diffusing pool fraction
FGT	=	Fibro glandular tissue
FoV	=	Field of view
in vivo	=	Experiments done on a whole living organism
$M_{\|\|}$	=	Component of magnetization parallel to main static field
$M_{\perp}$	=	Component of magnetization perpendicular to main static field
MR	=	Magnetic resonance
MP	=	Monopolar diffusion gradient
PAT	=	Parallel aquisition technique
PE	=	Phase encoding
RF	=	Radio frequency
RO	=	Read-out
ROI	=	Region of interest
SE	=	Spin echo
SPM	=	Statistical parametric mapping
SS	=	Slice selection
T_1	=	Spin-lattice relaxation time
T_2	=	Spin-spin relaxation time
t_d	=	Diffusion time
TE	=	Echo time
TM	=	Mixing time
TR	=	Repetition time
STEAM	=	Stimulated echo aquisition mode

Chapter 1

Introduction

Magnetic resonance imaging (MRI) is an integral part of modern medical diagnostics. In 2014, the average number of scans performed per 1000 in the EU was 67.5 [1]. The use of MRI is considered safe, with little to no side effects [2]. The use of the principle of magnetic resonance in imaging does not involve ionizing radiation, which its imaging counterparts computed tomography (CT) and positron emission tomography (PET) do [3, 4]. The versatility in the choice of what to image makes it an ubiquitous component of modern medicine. Through MRI it is possible to image magnetization relaxation, flow, and diffusion, among others. The aim of diffusion weighted imaging (DWI) is to monitor the random walks of molecules composing the object. Currently, DWI is the only noninvasive method available to study molecular displacements *in vivo* on length scales of micrometers. The ability of DWI to probe these length scales is valuable due to this also being the length scales of cells, the building blocks of biological tissue.

Chapter 2

Theory

2.1 The MR experiment

MRI imaging is based on measuring the effects produced by the interaction of nuclear spin and magnetic fields. For the majority of MR imaging in humans, the single proton nucleus of hydrogen is studied. When subjected to a strong external magnetic field, the proton spin will precess about the field direction. The basis of producing a detectable signal rests on the ability to perturb the precession of hydrogen spins by means of combinations of additional external magnetic fields [5, 6].

2.1.1 The precessional motion of magnetic moments

For the following discourse, the spin of a particle is described using a classical approach to electromagnetism. The quantum mechanical underpinnings of the behaviour of spins in magnetic fields is excluded for the sake of brevity.

In the presence of an external magnetic field $\vec{B}_0$, a magnetic moment will precess counter clockwise about the field direction, as shown in Figure 2.1. The equation of motion is given in Equation (2.1).

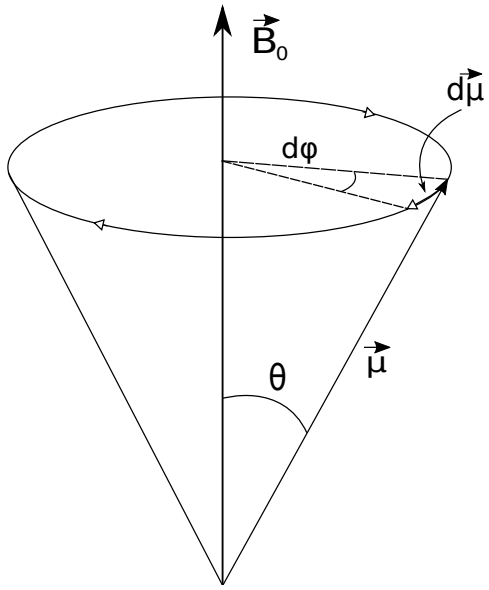

Figure 2.1: The precessional motion of a magnetic moment $\vec{\mu}$ in a magnetic field $\vec{B}_0$ is depicted in the figure. For the magnetic moment presented here, the precessional motion proceeds in a counter-clockwise manner.

$$\frac{d\vec{\mu}}{dt} = \gamma\vec{\mu} \times \vec{B} \tag{2.1}$$

The precession angular frequency for a magnetic moment in a external magnetic field is given in Equation (2.2), which is colloquially known as the Larmor equation.

$$\omega_0 = \gamma B_0 \tag{2.2}$$

2.1.2 Rotating reference frame

It is helpful to introduce the concept of a rotating reference frame when operating with precessional motion. In the laboratory frame, the precessional motion of a magnetic moment is pictured in Figure 2.1. For a reference frame which rotates counter-clockwise about the precessional axis at angular frequency ω_0, the magnetic moment vector will appear stationary. This simplifies the analysis of precessional motion. Equation (2.1) will be transformed to the following form

$$\frac{\partial\vec{\mu}}{\partial t} = 0 \tag{2.3}$$

where the use of $\frac{\partial}{\partial t}$ denotes here the rotating frame of reference.

2.1.3 Energy levels of proton spin states

The proton is a spin $1/2$ particle, which means the only available spin states will be parallel or anti-parallel with the external field. The energy difference is given in Equation (2.4), where $\hbar$ is the reduced Planck's constant and ω_0 is the Larmor frequency (Equation (2.2)).

$$\Delta E = \hbar\omega_0 \tag{2.4}$$

For hydrogen protons of water molecules, the gyromagnetic ratio γ has a value of $2.68 \times 10^8\,\mathrm{rad\,s^{-1}\,T^{-1}}$ or in terms of frequency: $\gamma/(2\pi) = 42.6\,\mathrm{MHz\,T^{-1}}$. For a modern 3 Tesla MR scanner, the precession frequency will be $127.8\,\mathrm{MHz}$. Figure 2.2 depicts the available spin states and energy difference between these states.

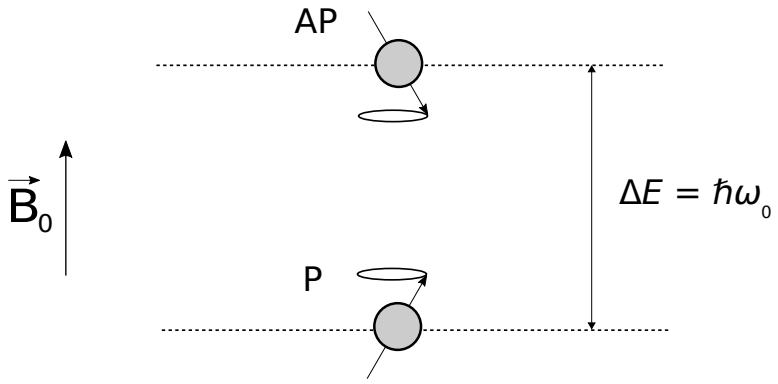

Figure 2.2: An anti-parallel (AP) orientation with respect to the field $\vec{B}_0$ of a spin is characterized by a energy difference given by ΔE compared to parallel (P) alignment of the spin.

2.1.4 Thermal energy considerations

Thermal energy associated with non-zero absolute temperature will prevent spins from relaxing completely, and thereby becoming fully parallel with the external field. In the range of human body temperature, the average thermal energy, kT, will be millions of times larger than the energy difference between parallel and anti-parallel alignment for the spin.

From Boltzman statistics, the population difference between two states can be calculated [7].

$$\frac{N_+}{N_-} = \exp(\frac{\hbar\omega_0}{kT}) \simeq 1 + \frac{\hbar\omega_0}{kT} \tag{2.5}$$

In Equation 2.5, N_+ and N_- represents the number of spins being parallel or anti-parallel to the external field, respectively. The Boltzmann constant is given by k and the temperature is given by T. From Equation (2.5) with $kT >> \hbar\omega_0$, the excess of spins being parallel to the external field is miniscule. The excess of parallel spins can be estimated using Equation (2.5). The spin excess is given in Equation 2.6.

$$\text{spin excess} \simeq N_- \frac{\hbar\omega_0}{kT} \simeq N \frac{\hbar\omega_0}{2kT} \tag{2.6}$$

The preference for parallel alignment is miniscule, but since N is on the order of Avogadros number ($\sim 10^{23}$) in typical experiments, the spin excess will be large enough to experimentally measurable.

2.1.5 Available equilibrium magnetization

The equilibrium magnetization can be calculated by multiplying the proton magnetic moment, $\gamma\hbar/2$, with the spin excess (Equation (2.6)) and the spin density, ρ_0. This is presented in Equation (2.7).

$$M_0 = \frac{\rho_0 \gamma^2 \hbar^2}{4kT} B_0 \tag{2.7}$$

M_0 in Equation 2.7 represent the available reservoar of magnetization which can be manipulated to give a measurable signal.

2.1.6 The magnetization vector

In the case of imaging of a macroscopic body, it is helpful to introduce the local magnetic moment per volume, the magnetization vector, $\vec{M}(\vec{r}, t)$. For a small volume element or voxel containing a large number of spins and where external fields can be considered constant throughout its volume, the magnetization can be given as a sum of the spins.

$$\vec{M} = \frac{1}{V} \sum_{\text{spin } i} \vec{\mu}_i \tag{2.8}$$

The set of spins $\vec{M}$ in the volume V is called an spin isochromat, which is defined as an ensemble of spins precessing with the same phase. An illustration of $\vec{M}$ is given in Figure 2.3.

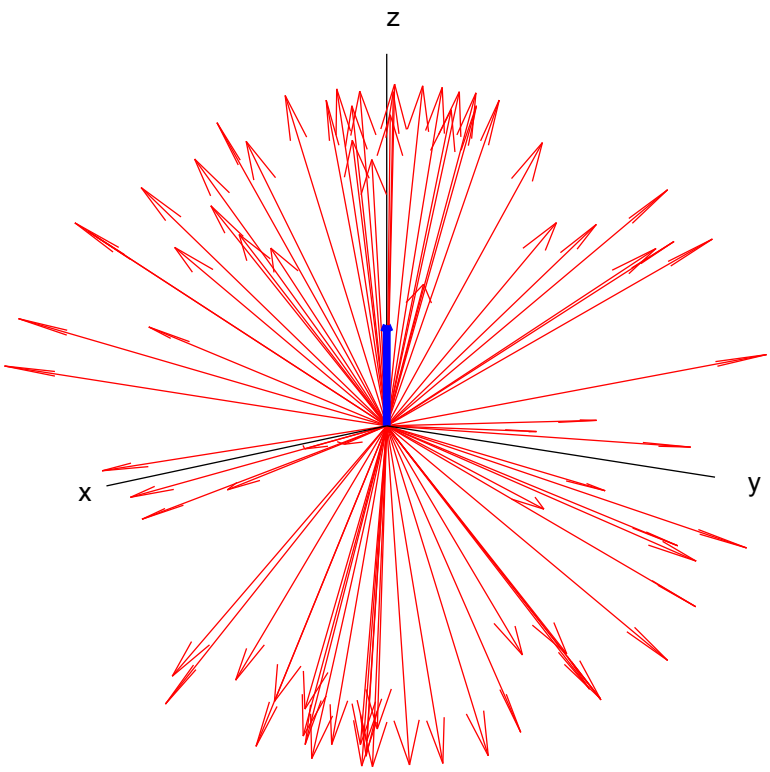

Figure 2.3: The magnetization vector is the sum of many magnetic moments. In the presence of a magnetic field, there will be a preferential alignment of spins. This excess of spins is represented by the magnetization. In the figure, red arrows represents magnetic moments. The blue arrow represents the magnetization. For an unperturbed system (being in equilibrium with its surroundings), the magnitude of the magnetization vector will be equal to the equilibrium magnetization given in Equation 2.7.

2.1.7 Magnetization of non-interacting spins

For non-interacting spins, the equation of motion of a single spin (Equation (2.1)) can be used to describe the behaviour of the spin ensemble. This is represented in Equation (2.9).

$$\frac{1}{V}\sum_i \frac{d\vec{\mu}_i}{dt} = \frac{\gamma}{V}\sum_i \vec{\mu}_i \times \vec{B}_{ext} \tag{2.9}$$

or by using Equation (2.8)

$$\frac{d\vec{M}}{dt} = \gamma \vec{M} \times \vec{B}_{ext} \quad , \quad \text{(non-interacting spins)} \tag{2.10}$$

A common coordinate system used in MRI is to set the direction $\hat{z}$ to be along the main magnetic field. From this, the directions $\hat{x}$ and $\hat{y}$ lie in the plane transverse to the main

magnetic field. Suppose a static magnetic field is applied along one direction, $\vec{B}_{ext} = B_0\hat{z}$. Then the magnetization vector can be represented in terms of its component parallel and perpendicular to the field $\vec{B}_{ext}$. Here, the parallel component is given by

$$M_{||} = M_z \tag{2.11}$$

and the perpendicular components are

$$\vec{M}_{\perp} = M_x\hat{x} + M_y\hat{y} \tag{2.12}$$

The transverse perpendicular magnetization can also be rewritten in complex terms as in Equation (2.13).

$$M_+(t) \equiv M_x(t) + iM_y(t) \tag{2.13}$$

Equations (2.11) and (2.12) can be used to decouple the magnetization vector given in Equation (2.10). The equations of motion for the parallel and perpendicular components of the magnetization vector are given in Equations (2.14) and (2.15).

$$\frac{dM_z}{dt} = 0 \quad , \quad \text{(non-interacting spins)} \tag{2.14}$$

$$\frac{d\vec{M}_{\perp}}{dt} = \gamma\vec{M}_{\perp} \times \vec{B}_{ext} \quad , \quad \text{(non-interacting spins)} \tag{2.15}$$

2.1.8 RF pulses

In order to study the magnetization vector, it must be perturbed from its equilibrium value. This can be done by applying a radiofrequency (RF) pulse in the transverse plane. This pulse is denoted by $\vec{B}_1$. This pulse is set to oscillate at the Larmor frequency. In the rotating reference frame $\vec{B}_1$ will be stationary and it will cause the magnetization vector to precess about it, as seen from Equation 2.1. By only applying the pulse for a set amount of time, the magnetization vector may be tipped into the transverse plane. Common RF pulses are a 90° pulse, wherby the magnetization is moved into the transverse plane assuming it previously resided longitudinally. An 180° pulse serves the purpose of inverting the magnetization. This pulse is used in generating spin echoes and performing inversion recovery experiments.

2.1.9 T_1 relaxation

Equation (2.14) describes the behaviour of the longitudinal magnetization for non-interacting spins. Suppose the equilibrium magnetization (Equation (2.7)) is perturbed by some additional magnetic field such as an RF pulse. Following this perturbation, the magnetization is expected to attempt to regain its equilibrium value, by way of spins interacting their surroundings. The rate of change of the longitudinal magnetization is proportional to the difference between the equilibrium value and its current value ($M_0 - M_z$). The regrowth of longitudinal magnetization is given in Equation (2.16).

$$\frac{dM_z}{dt} = \frac{1}{T_1}(M_0 - M_z) \tag{2.16}$$

where T_1 is the spin-lattice relaxation time. Equation (2.16) can be solved, and the solution is given in Equation (2.17).

$$M_z(t) = M_z(0)\exp(-t/T_1) + M_0(1 - \exp(-t/T_1)) \tag{2.17}$$

The behaviour of the longitudinal magnetization is depicted in Figure 2.4.

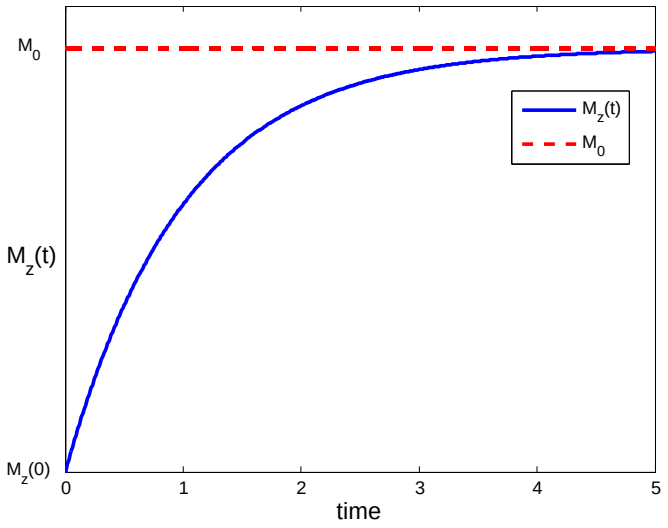

Figure 2.4: Following a pertubation of the magnetization vector, the longitudinal component of magnetization will move towards its equilibrium value. At a time T_1 following a pertubation which left $M_z(0) = 0$, the longitudinal magnetization is 63% of its equilibrium value.

2.1.10 T_2 relaxation

The decay of transverse magnetization can be understood from how the magnetization vector is defined. It is a sum of many magnetic moments, which vector sum forms the magnetization vector. In the transverse plane, these moments will be subjected to both the magnetic field of its immediate neighborhood and the applied magnetic field. The magnetic field from neighbooring moments combined with non-perfect homogeniety of the main field will result in isochromats being subjected to differing magnetic fields. The precessional frequency is given by the Larmor equation (Equation (2.2)), and these differing magnetic fields will lead to differing precessional frequency. The result of this is the decay of the transverse component of the magnetization vector due to the relative dephasing of its comprising magnetic moments.

The overall relaxation time parameter, which includes the effects of static and dynamic dephasing, is represented by T_2^*. The relationship between T_2^* and static and dynamic dephasing is shown in Equation (2.18).

$$\frac{1}{T_2^*} = \frac{1}{T_2'} + \frac{1}{T_2} \tag{2.18}$$

The relaxation times can also be expressed in terms of rates, as given in Equation (2.19).

$$R_2^* = R_2' + R_2 \tag{2.19}$$

In Equation (2.19), T_2' quantifies the dephasing due to external field inhomogeneities, and T_2 quantifies the dephasing due to dynamic effects such as rapidly fluctuating neighboorhood fields. For a spin-echo experiment, the effects of T_2'-decay may be suppressed, so only the effect of dynamic dephasing affect the decay of the transverse magnetization. The parameter T_2 is called the spin-spin relaxation time.

The decay of transverse magnetization for the lab frame of reference and rotating frame of reference is given in Equation (2.20) and Equation (2.21), respectively. In Figure 2.12, the decay of the magnitude of the transverse magnetization is presented.

$$\frac{d\vec{M}_\perp}{dt} = \gamma \vec{M}_\perp \times \vec{B}_{ext} - \frac{1}{T_2}\vec{M}_\perp \tag{2.20}$$

$$\frac{\partial \vec{M}_\perp}{\partial t} = -\frac{1}{T_2}\vec{M}_\perp \tag{2.21}$$

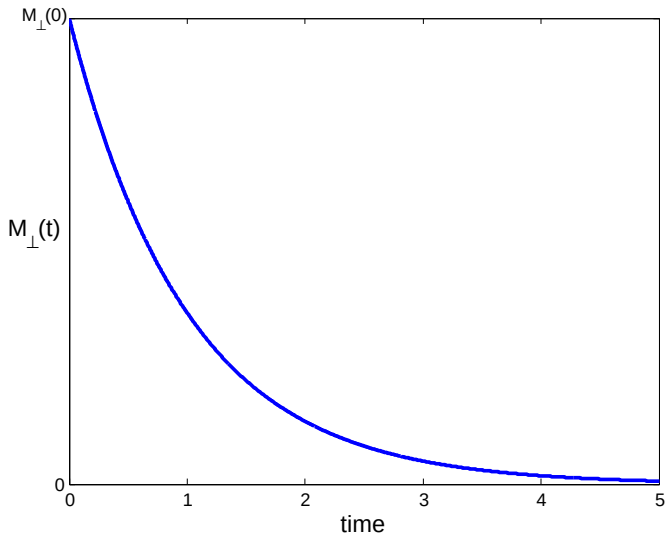

Figure 2.5: Due to dephasing, the transverse magnetization will decay exponentially from its initial value $M_\perp(0)$. For a spin-echo experiment, after some time T_2, the transverse magnetization will have decayed to 37% of its initial value.

2.2 The Bloch-Torrey equation

The effects of T_1 and T_2 relaxation can be combined in a vector equation, the Bloch-Torrey equation.

$$\frac{d\vec{M}}{dt} = \gamma\vec{M} \times \vec{B}_{ext} + \frac{1}{T_1}(M_0 - M_z)\hat{z} - \frac{1}{T_2}\vec{M}_{\perp} \tag{2.22}$$

Equation (2.22) can be solved by first expanding the cross product term and integrating. Assuming $\vec{B}_{ext} = B_0\hat{z}$, the component wise solutions of Equation (2.22) are given in Equations (2.23), (2.24) and (2.25).

$$M_x(t) = e^{-t/T_2}(M_x(0)\cos(\omega_0 t) + M_y(0)\sin(\omega_0 t)) \tag{2.23}$$

$$M_y(t) = e^{-t/T_2}(M_y(0)\cos(\omega_0 t) - M_x(0)\sin(\omega_0 t)) \tag{2.24}$$

$$M_z(t) = M_z(0)e^{t/T1} + M_0(1 - e^{-t/T_1}) \tag{2.25}$$

An illustration of the behaviour of the magnetization vector in the laboratory frame is shown in Figure 2.6. Here, the magnetization vector is initially displaced from equilibrium and is placed along the y-axis. After this, the transverse compontent can be seen to precess, while being damped by the factor involving T_2 before finally approaching zero in magnitude. The regrowth of the longitudinal component is observed, and is goverened by the T_1 relaxation time.

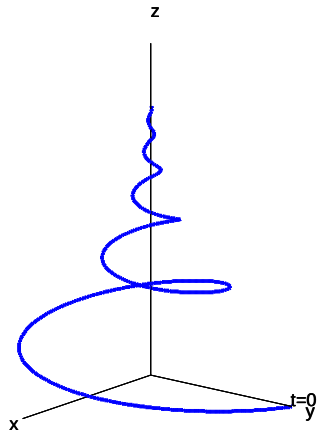

Figure 2.6: The relaxation of the magnetization vector in the laboratory frame, following an initial pertubation which aligns the magnetization vector with the y-axis. Over time, the magnetization vector approaches its equilibrium value along the z-axis, assuming the static field is given by $\vec{B}_{ext} = B_0\hat{z}$.

The complex representation of transverse magnetization as given in Equation (2.13) can be used to combine the solutions given in Equation (2.23) and (2.24).

$$M_+(t) = M_\perp e^{i\phi(t)} \quad , \quad \phi(t) = -\omega_0 t + \phi(0) \tag{2.26}$$

Noting that the magnitude of $M_+(t)$ equals $M_\perp(t)$.

2.3 Spatial encoding in MRI

Magnetic field gradients are used to spatially encode the signal from an object in order to produce an image. This is done by applying an additional magnetic field which is parallel to the main magnetic field, but varies linearly based on position. By applying a slice selection gradient G_{SS} in some direction simultaneously with the application of an RF pulse, only a slice of the object perpendicular to G_{RO} will be excited.

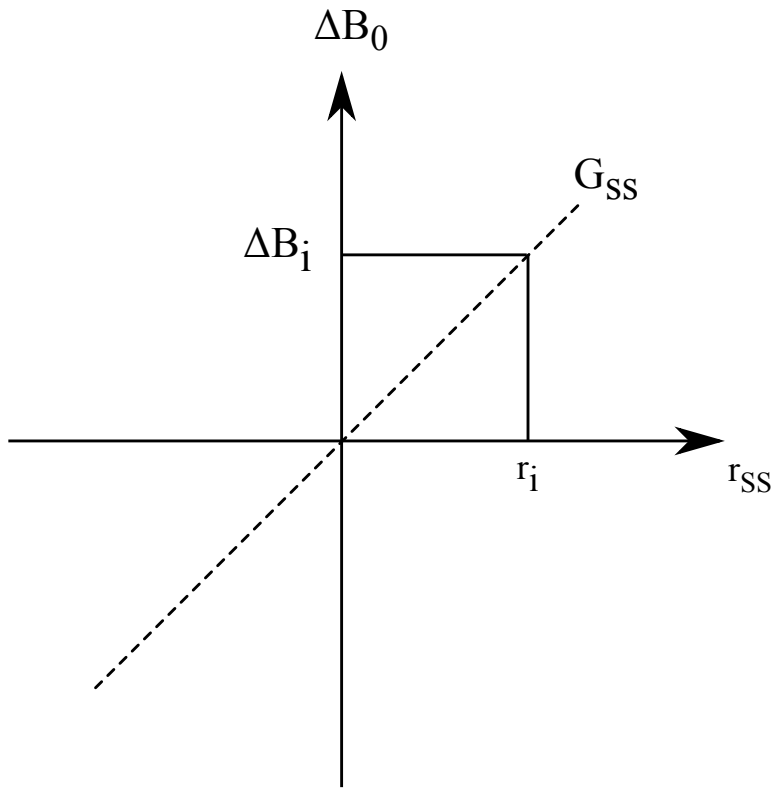

Figure 2.7: The appliction of a slice selection gradient along some direction r_{ss} will cause the effective magnetic field to vary based on position, and thereby varying precessional frequency based on position. By tuning the RF pulse to oscillate at a frequency specified by ΔB_i, only spins in the plane perpendicular to r_i will be excited.

Following the exitation of the slice, two perpendicular gradients, G_{RO} and G_{PE} are applied in the plane of excitation, along the *read out* (RO) and *phase encoding* (PE) directions. Setting x as the RO direction and y as the PE direction, the signal from the exited slice of an object may be expressed as

$$S(t) \propto \int\int_{slice} M_{\perp}(x,y) e^{-2\pi(k_x x + k_y y)} dk_x dk_y \tag{2.27}$$

In Equation 2.27, $k_{x,y}(t) = \frac{\gamma}{2\pi} \int_0^t G_{x,y}(t')dt'$. By registering the signal over time as the gradients are carefully applied, an image in *k-space* is formed. The actual magnetization can be obtained by two dimensional inverse Fourier transform of the k-space image. In echo planar imaging (EPI), the whole k-space or a large portion is registered from one spin-echo. In Figure 2.8, the measurement trajectory in k-space is illustrated.

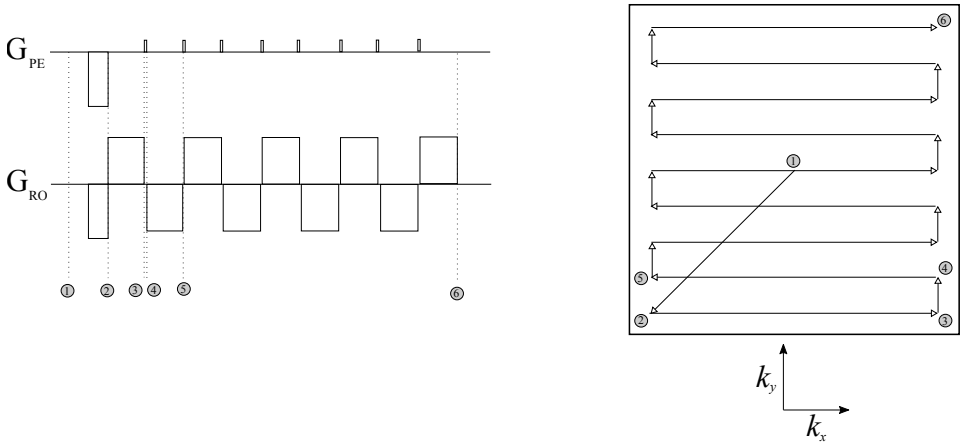

Figure 2.8: By the application of gradients at specific intervals and duration, it is possible to register an MR signal as a function of one variable (time) and subsequently, using transforms, producing a two dimensional image, which by definition is characterized by two variables.

2.4 The MR experiment and diffusion

The manifestation of molecular movement in the form of Brownian motion or diffusion will have an effect on the MR experiment. Diffusion is a type of transport process which does not require bulk motion to move particles from one location to another. This property separates diffusion from convection and dispersion, two other important transport processes. The process of diffusion is based on the phenomenon of particles in solution moving from areas of high particle concentration to low concentration. This physical phenomenon is described by Fick's first law, shown in Equation (2.28).

$$\vec{J} = -D\nabla n \tag{2.28}$$

In Equation (2.28), $\vec{J}$ is the net particle flux vector and ∇n is the gradient of the particle concentration.The process is illustrated in Figure 2.9.

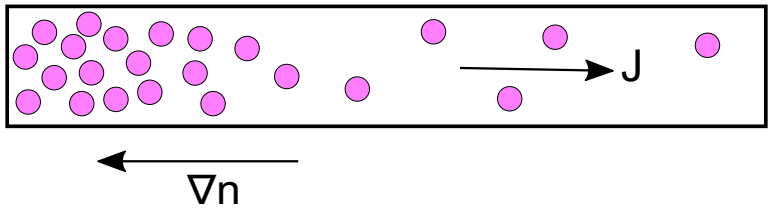

Figure 2.9: Particles in solution move from regions of high concentration to low concentration. $\vec{J}$ is the net particle flux and ∇n is the gradient of the particle concentration.

Furthermore, conservation of total particle number requires that the time rate of change of n is related to the flux divergence as given in Equation (2.29).

$$\frac{\partial n}{\partial t} = -\nabla \cdot \vec{J} \tag{2.29}$$

Combining Equations (2.28) and (2.29) give the diffusion equation, given in Equation (2.30). This relationship is also known as Fick's second law.

$$\frac{\partial n}{\partial t} = D\nabla^2 n \tag{2.30}$$

Fick's laws describes the consequence of having a nonuniform concentration of a solute particle or molecule. Over time, the particles or molecules will seek to nullify concentration gradients. Einstein suggested Fick's laws also were applicable to the process of self-diffusion. A water molecule diffusing in water is an example of self diffusion. In order to describe the motion of particles by self-diffusion, the conditional probability $P(\vec{r}|\vec{r'}, t)$ is introduced. P gives the probability of a particle at $\vec{r}$ at time zero moving to $\vec{r'}$ after some time t. With this, n can now be thought of as the probability of observing a particle at a location $\vec{r'}$ after some time t.

$$n(\vec{r'}, t) = \int n(\vec{r}, 0) P(\vec{r}|\vec{r'}, t) \tag{2.31}$$

$n(\vec{r'}, t)$ obeys the diffusion equation for arbitary initial conditions, therefore the conditional probability $P(\vec{r'}|\vec{r}, t)$ obeys the diffusion equation as well.

$$\frac{\partial P(\vec{r}|, \vec{r'}, t)}{\partial t} = D\nabla^2 P(\vec{r}|\vec{r'}, t) \tag{2.32}$$

Choosing the initial condition where all particles start at some position $P(\vec{r}|\vec{r'}, t) = \delta(\vec{r'} - \vec{r})$, the solution for Equation (2.32) is a Gaussian function, given in Equation (2.33).

$$P(\vec{r}|\vec{r'}, t) = \frac{1}{(4\pi Dt)^{3/2}} \exp(-\frac{(\vec{r'} - \vec{r})^2}{4Dt}) \quad , \quad \text{for three dimensions} \tag{2.33}$$

Einstein's equation for diffusion can be obtained by computing the ensemble average of $(\vec{r'} - \vec{r})^2$ in Equation (2.33).

$$< \left(\vec{r'} - \vec{r}\right)^2 >= 6Dt \tag{2.34}$$

2.4.1 The pulsed gradient spin-echo (PGSE) experiment

The motion of spins can be detected in MRI by using magnetic field gradients. Suppose a magnetic field gradient is applied after the magnetization has been turned into the transverse plane by way of a 90° pulse. This gradient is turned on for some short time δ. This gives the spins a phase change based on position. The phase change will be

$$\phi_1 = -qx_1 \tag{2.35}$$

where $q = \gamma\delta G$.

For this the narrow-pulse approximation is used, whereby it is assumed that no diffusion takes place during the application of the gradient. After some time a $180°$ refocusing RF pulse is applied. Following this a secondary diffusion gradient pulse is applied. This pulse seeks to cancel the phase change aquired by spins during the first pulse. The total phase change is given in Equation (2.36).

$$\Delta\phi = \phi_2 - \phi_1 = -q(x_2 - x_1) \tag{2.36}$$

If the spins are diffusing, there will be a non-zero aquired phase, which will attenuate the signal due to dephasing. If, on the other hand, the spins are stationary, then the phase change will be zero, thus not attenuating the aquired signal.

A simple diagram of the diffusion sequence is presented in Figure 2.10 [8].

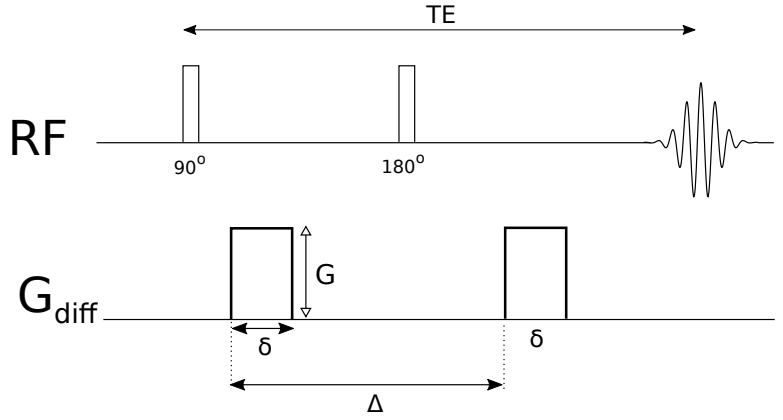

Figure 2.10: An initial 90^o-pulse is applied to tilt the magnetization vector into the transverse plane. Following this is the application of the first diffusion gradient. This pulse encodes the position of spins through their phase. A 180^o RF refocusing pulse inverts the phase of the spin population before the decoding diffusion pulse is applied. The polarity of the diffusion pulses are the same due to the use of a 180^o RF refocusing pulse.

Diffusion in an object can be probed by the use of gradients and its effect can be studied using the Bloch-Torrey equation (Equation (2.22)). For the sake of brevity excluding T_1 and T_2 relaxation effects, the Bloch-Torrey equation in the rotating frame is

$$\frac{\partial \vec{M}(\vec{r},t)}{\partial t} = \gamma \vec{M}(\vec{r},t) \times \vec{B} + D\nabla^2 \vec{M}(\vec{r},t) \quad , \quad \vec{B} = (\vec{G}\cdot\vec{r})\hat{z} \tag{2.37}$$

In Equation (2.37), the diffusion gradient magnetic field is represented by $\vec{B}$. The application of this gradient will affect the phase of spins depending on position. For this case, where only the phase of spins is affected, the complex representation of the transverse magnetization (Equation (2.26)) is used in solving Equation (2.37). The substitution is performed:

$$\frac{\partial M_+(\vec{r},t)}{\partial t} = \gamma(\vec{r}\times\vec{G})M_+(\vec{r},t) + D\nabla^2 M_+(\vec{r},t). \tag{2.38}$$

For the case of no diffusion, $D = 0$, the solution of Equation (2.38) is

$$M_+(\vec{r},t) = A\exp(-i\gamma\vec{r}\cdot\int_0^t \vec{G}(t')dt') \tag{2.39}$$

To solve for thecase where (spatially invariant) diffusion is present, A from Equation (2.39) is assumed to be a function of time, $A = A(t)$. Using the solution given in Equation (2.39):

$$\frac{\partial A(t)}{\partial t} = \exp\left(i\gamma\vec{r}\cdot\int_0^t \vec{G}(t')dt'\right) D\nabla^2 M_+(\vec{r},t) \tag{2.40}$$

By using the relationship of differentiation of the logarithm of a function, $\frac{1}{A(t)}\frac{\partial A(t)}{\partial t} = \frac{\partial}{\partial t}\ln A(t)$, Equation (2.41) is obtained.

$$\frac{\partial}{\partial t}\ln A(t) = D\exp\left(i\gamma\vec{r}\cdot\int_0^t \vec{G}(t')dt'\right)\nabla^2\left[\exp\left(-i\gamma\vec{r}\cdot\int_0^t \vec{G}(t')dt'\right)\right] \tag{2.41}$$

Equation (2.41) can be solved by assuming $A(0) = 1$, giving the Equation (2.42).

$$\ln A(t) = -D\gamma^2\int_0^t dt''\left[\left(\int_0^{t''}\vec{G}(t')dt'\right)^2\right] \tag{2.42}$$

From the above solution, it can be observed that the diffusion coefficient D is accessible through an experimental setup through the diffusion gradient $\vec{G}$. From Equation (2.42), the b-value can be defined.

$$b = \gamma^2\int_0^t dt''\left[\left(\int_0^{t''}\vec{G}(t')dt'\right)^2\right] \tag{2.43}$$

For a pulse sequence such as presented in Figure 2.10, the b-value can be calculated to be

$$b = \gamma^2 G\delta^2(\Delta - \frac{\delta}{3}) \tag{2.44}$$

2.5 Stimulated echo aquisition mode (STEAM)

An inherent issue of performing diffusion measurements at higher diffusion times is increasing significance of T_2-decay. The signal may decay to unrecoverable levels, rendering image formation unavailable. A way to explore longer diffusion times is given by stimulated echo sequences, also known as STimulated Echo Aquisition Mode, or STEAM [9]. The principle underlying these techniques is to store a transverse coherence pathway in the longitudinal direction for a some time known as the mixing time (*TM*). While stored in the longitudinal direction, the spins composing the coherence pathway will be governed by T_1 signal decay. Longitudinal T_1 signal decay is for many substances much less compared to transversal T_2 decay. A drawback of STE sequences is a reduction of available magnetization/signal by about a half compared to regular echo sequences. Undesirable coherence pathways are completely dephased by using special crusher gradients. These other pathways would otherwise influence the eventual stimulated echo. A sequence diagram of a stimulated echo sequence is given in Figure 2.11.

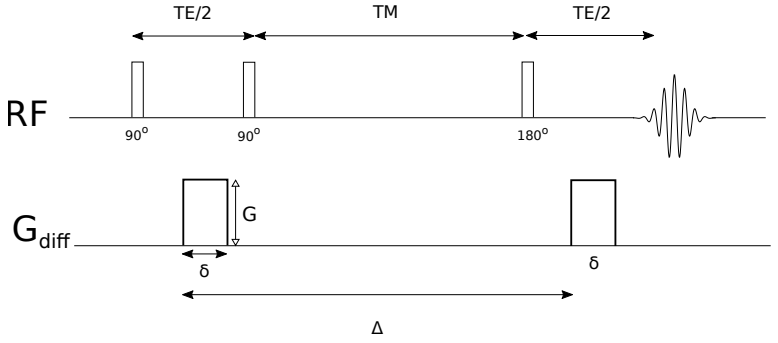

Figure 2.11: For the STEAM sequence, the magnetization is tilted to the transverse plane before being subjected to the primary diffusion encoding pulse. Following this a 90^o RF pulse tilts a fraction of the magnetization to the longitudinal direction. This fraction continues to precess and diffuse, while the decay is modulated by T_1-decay. After a time interval given as the mixing time (*TM*), another 90^o pulse is used to move this fraction of magnetization into the transverse plane. Following the second diffusion gradient pulse, the fraction of the magnetization following the same coherence pathway forms a stimulated echo.

2.6 Oscillating diffusion sequences

Imaging at sufficient short diffusion times will in principle allow for measurement of the intrinsic diffusion coefficient. At short enough diffusion times, the reduction of ADC due to restriction will not have manifested itself. In MRI, limitations on gradient strengths prohibit

the application of sufficiently short pulses to explore this short diffusion time regime *in vivo*. A way to reach these short diffusion times is to apply oscillating diffusion gradients [10]. In this modality, a succession of diffusion weighting periods is implemented. The concept of diffusion time is complicated, as a diffusion spectrum is aquired rather than a single scalar value.

2.7 Bipolar diffusion gradients

Bipolar gradients may be used to lessen the image artifacts produced by incompletely canceled eddy currents in echo planar imaging [11]. A bipolar diffusion sequence is presented in Figure 2.12. The diffusion weighting supplied by using a bipolar diffusion sequence is less than compared to a monopolar scheme. With equal pulse width δ, the effective b value of a bipolar sequence is less than 25% compared to the monopolar sequence. This leads to drawbacks such as increasing the minimum echo time compared to monopolar sequences, due to requiring longer δ's to achieve the same b-value.

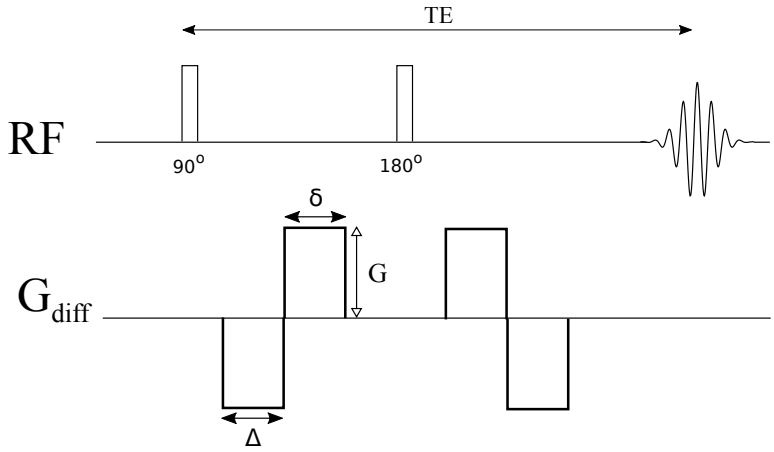

Figure 2.12: A bipolar diffusion sequence is presented. Δ is the duration of the first lobe [11], and δ is the duration of the second.

2.8 Biophysical models describing relaxation-diffusion

2.8.1 Slow exchange

A system which consists of two populations of spins which experience no exchange, can be modeled by a biexponential function. This is given in Figure (2.45). In this model, f represents the fraction of signal arising from the fast diffusing compartment. The biexponential model has been used to classify the deviation from monoexpoential decay which appears at high b-values for tissues. The common biophysical interpretation of this model is that the fast diffusing pool is the extracellular water content, which is less restricted

than the slowly diffusing pool. This pool is viewed as the water which is contained in cells, which is by this trapped in a container, thus limiting diffusion[12].

$$S(TE,b) = S_0\left(fe^{-b\cdot ADC_{\text{fast}}}e^{-TE/T_{2,\text{fast}}} + (1-f)e^{b\cdot ADC_{\text{slow}}}e^{-TE/T_{2,\text{fast}}}\right) \quad , \quad 0 < f < 1 \tag{2.45}$$

An alternative to the biexponential model in the case of slow exchange is the following. Assuming monoexponential signal decay along the axes of both diffusion and relaxation, the signal may be modeled as Equation (2.46).

$$S(TE,b) = S_0 e^{-b\cdot ADC_{\text{effective}}}e^{TE/T_{2,\text{effective}}} \tag{2.46}$$

where

$$ADC_{\text{effective}} = f\cdot ADC_{\text{fast}} + (1-f)ADC_{\text{slow}}$$

and

$$\frac{1}{T_{2,\text{effective}}} = f\frac{1}{T_{2,\text{fast}}} + (1-f)\frac{1}{T_{2,\text{slow}}}$$

If f is an experimental parameter, then ADCslow and $T_{2,\text{slow}}$ can be approximated.

2.8.2 Fast exchange

If the pools exchange spins as is facilitated by transport proteins in cellular membranes in cells, then the signal behaviour will be different compared to the model presented in Equation 2.45. For the case of fast exchange between pools, a monoexponential decay along the axis of TE and b will be experienced as outlined above. The difference is now the modification of f in the model.

For the case of diffusion as given in Equation (2.47):

$$S(b) = S_0 e^{-b\cdot ADC_{\text{effective}}} \tag{2.47}$$

where

$$ADC_{\text{effective}} = f_{\text{fast}}ADC_{\text{fast}} + f_{\text{slow}}ADC_{\text{slow}}$$

and

$$f_{\text{fast}} = \frac{fe^{TE/T_{2,\text{fast}}}}{fe^{TE/T_{2,\text{fast}}} + (1-f)e^{TE/T_{2,\text{slow}}}} \quad , \quad f_{\text{fast}} + f_{\text{slow}} = 1$$

f is here the original fast diffusing pool fraction. Conversely, relaxation with fast exchange can be modelled by Equation 2.48.

$$S(TE) = S_0 e^{TE/T_{2,\text{effective}}} \tag{2.48}$$

where

$$\frac{1}{T_{2,\text{effective}}} = f_{\text{fast}}\frac{1}{T_{2,\text{fast}}} + f_{\text{slow}}\frac{1}{T_{2,\text{slow}}}$$

and

$$f_{\text{fast}} = \frac{fe^{-b\cdot ADC_{\text{fast}}}}{fe^{-b\cdot ADC_{\text{fast}}} + (1-f)e^{-b\cdot ADC_{\text{slow}}}}$$

In describing the relaxation-diffusion signal in this manner, it is of great simplification if one of the processes is represented by slow exchange and the other by fast exchange. If this is the case, then the calculation of the updated volume fractions f_{fast} and f_{slow} will be straightforward. Fast exchange is represented by a change in $T_{2,\text{effective}}$ when varying b, and, a change in $ADC_{\text{effective}}$ when changing TE. Slow exchange is characterized by the absence of this dependency. Both processes are dependent then the situation is complicated.

2.9 Bakers yeast

Baker's yeast is a common strain of the yeast species *Saccharomyces cerevisiae*. The cells have a diameter of $5\,\mu\text{m}$ to $10\,\mu\text{m}$, and have the shape of spheres or ovoids [13].

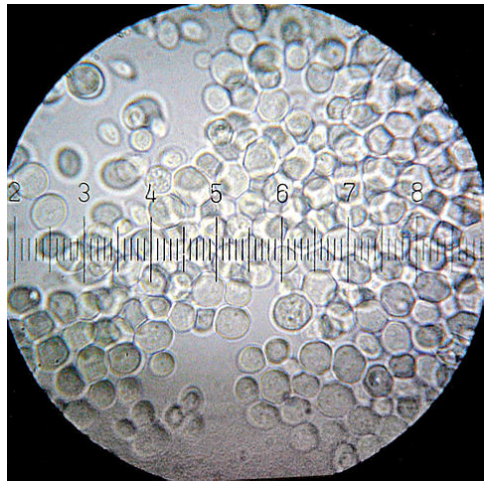

Figure 2.13: A microscopy image of Baker's yeast. Gradation marks in the reticle are of $1\,\mu\text{m}$[14].

2.10 Breast tissue

The female breast consist of two major tissue types: Fibroglandular tissue and adipose tissue [15]. In an MRI experiment of breast tissue, the need to suppress the signal arising from fat is important. Common techniques to accomplish this is fat saturation, inversion recovery and opposed-phase imaging [16].

Figure 2.14: Illustration of breast tissue structures[17]. The center part of the breast constitutes of what can be classified as fibroglandular tissue. This includes milk glands, milk ducts and supportive tissue. Surrounding the tissue and colored in yellow are adipose tissue.

Chapter 3

Methods

The MR measurements collected were aquired by a 3 T MAGNETOM PRIMA scanner (Siemens Healthcare, Erlangen, Germany)[18]. Specifications of the scanner system is given in Table 3.1.

Table 3.1: Technical details of the Siemens 3 Tesla Prisma scanner.

Field strength	3 Tesla
Bore size	60 cm
System length	213 cm
Maximum gradient strength	80 mT/m
Gradient slew rate	200 mT/m/s

3.1 Yeast solution scan, April 28 2017

Packets of $50\,\mathrm{g}$ bakers yeast (Saccharomyces cerevisiae) were bought from the local store. These packets were suspended using set amounts tap water at room temperature. Three different mixing fractions were prepared $f = 0.5$,0.43 and 0.33, where f symbolizes the water fraction of the solution prepared: $f = 0.5 = \frac{100\,\mathrm{g\ water}}{200\,\mathrm{g\ total}} = \frac{100\,\mathrm{g\ water}}{100\,\mathrm{g\ water}+100\,\mathrm{g\ yeast}}$. Subsequently, the solutions were subjected to diffusion MRI scans as detailed in Table 3.2.

Table 3.2: Yeast scan sequence specifics. Monopolar (MP) and bipolar (BP) diffusion gradients were applied. Spin echo (SE) were used for producing detectable signal.

Seq. type	TR (ms)	TE (ms)	t_d (ms)	b (s/mm^2)	Other
MP SE	5300	53	14.8	0 150 550	
MP SE	6800	100	14.8	0 150 550	
MP SE	6800	100	65.9	0 150 550	
BP SE	5700	75	8.6	0 150 550	
MP STEAM	5700	64	197.4	0 150 550	$T_{mix} = 177\,\mathrm{ms}$
Sine diff. grad. SE	5800	77	7.1	0 150 550	$f = 50\,\mathrm{Hz}$
Cosine diff. grad. SE	7300	111	6.5	0 150 550	$f = 30\,\mathrm{Hz}$

Table 3.3: Specifics of yeast scan.

Directions	6
Averages per direction	2
Bandwith (Hz/pixel)	2200
FoV Read (mm)	340
FoV Phase (%)	47.1
Voxel dimension (xyz mm)	2x2x2.5
PAT factor	6
Partial fourier	6/8
Echo spacing (ms)	0.58
Slices	SE: 60 STEAM: 28

3.2 Volunteer scans

Scans of two healthy volunteers were performed on March 21 and May 9 2017. Before commencement of scans, the volunteers were informed about safety procedures by the radiographer present. During the scans, the volunteers lay prone and an MRI breast coil was used for signal aqusition. Total scan time for each volunteer was approximately one hour, including time spent preparing and minor delays during scan.

3.2.1 Volunteer scans I, March 21 2017.

Table 3.4: Volunteer scan I sequence specifics.

Seq. type	TR (ms)	TE (ms)	t_d (ms)	b (s/mm^2)	Other
MP SE	5300	41	15.8	0 150 450 700 1200	
MP SE	5300	85	15.8	0 150 450 700 1200	
MP SE	5300	85	63.5	0 150 450 700 1200 1800 2400 3000	
MP STEAM	5300	85	196.8	0 150 450 700 1200 1800 2400 3000	TM = 136.5 ms
Sine diff. grad. SE	5300	41	7.1	0 150 450 700	$f = 50\,\mathrm{Hz}$

Table 3.5: Specifics of volunteer scan I.

Directions	6
Averages per direction	2
Bandwith (Hz/pixel)	2200
FoV Read (mm)	340
FoV Phase (%)	47.1
Voxel dimension (xyz mm)	2x2x2.5
PAT factor	6
Partial fourier	6/8
Echo spacing (ms)	0.58
Slices	SE: 60 STEAM: 28

3.2.2 Volunteer scans II, May 9 2017.

Table 3.6: Volunteer scan II sequence specifics.

Seq. type	TR (ms)	TE (ms)	t_d (ms)	b (s/mm^2)	Other
MP SE	7300	53	14.8	0 150 550	
MP SE	7300	100	14.8	0 150 550	
MP SE	7300	100	65.9	0 150 550	
BP SE	7300	75	8.6	0 150 550	
MP STEAM	7300	54	197.4	0 150 550	TM = 177 ms
Sine diff. grad. SE	7300	77	7.1	0 150 550	$f = 50\,\mathrm{Hz}$
Cosine diff. grad. SE	7300	111	6.5	0 150 550	$f = 30\,\mathrm{Hz}$

Table 3.7: Specifics of voluteer scan II

Directions	12
Averages per direction	1
Bandwith (Hz/pixel)	794
FoV Read (mm)	340
FoV Phase (%)	47.1
Voxel dimension (xyz mm)	2x2x2.5
PAT factor	4
Partial fourier	6/8
Echo spacing (ms)	1.34
Slices	SE: 60 STEAM: 28

3.3 Image processing

Image files were processed using MATLAB [19] software and Statistical Parametric Mapping (SPM12) [20]. In MATLAB a program named MRIPSTO2 [21] was used to select regions of interest. Due to the exponential nature of MR signals, the ROIs from all directions were averaged geometrically. Averaging the intensity in a ROI were done arithmetically. Some images were delivered as in mosaic formats, which entailed that all the image slices comprising the object taken at some TE and b were delivered in one large image. For these,

SPM12 was used to split the mosaic image into its constituents. Analysis and model fitting were done in MATLAB, primarily using functions such as `polyfit` for simple regression and `fit` for model fitting. The ADC value used in analysis was the gradient coefficient obtained from fitting a straight line onto the ln transformed signal as a function of b. The range of b used in calculating ADC was for the yeast samples and volunteer scans in the month of March was b = 0, 150, 450, $700\,\mathrm{s/mm^2}$. For the volunteer scans performed in May, b = 0, 150, $550\,\mathrm{s/mm^2}$.

Chapter 4

Results

4.1 Volunteer A

4.1.1 T_2 for each b, ADC for each TE, ADC for each t_d

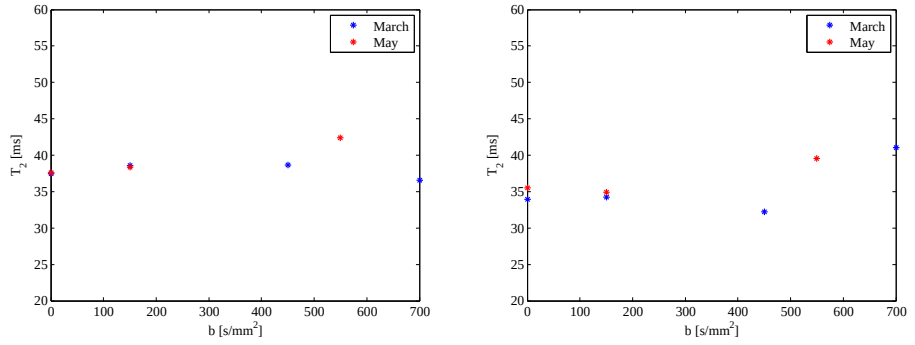

(a) Left breast

(b) Right breast

Figure 4.1: The measured T_2 values of left (4.1a) and right (4.1b) breast for different b-values for volunteer A. The measurements for both sessions are included in the figures. For March: t_d = 15.8 ms. For May t_d = 14.8 ms.

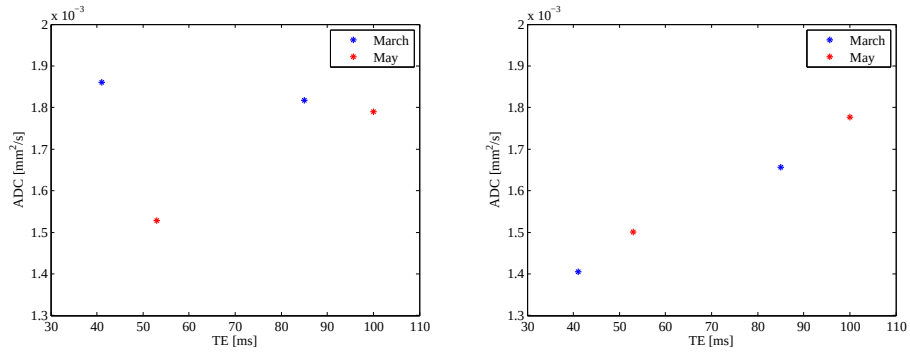

(a) Left breast **(b)** Right breast

Figure 4.2: The measured ADC values of left (4.2a) and right (4.2b) breast for different TE for volunteer A. The measurements for both sessions are included in the figures. For March: t_d = 15.8 ms. For May t_d = 14.8 ms.

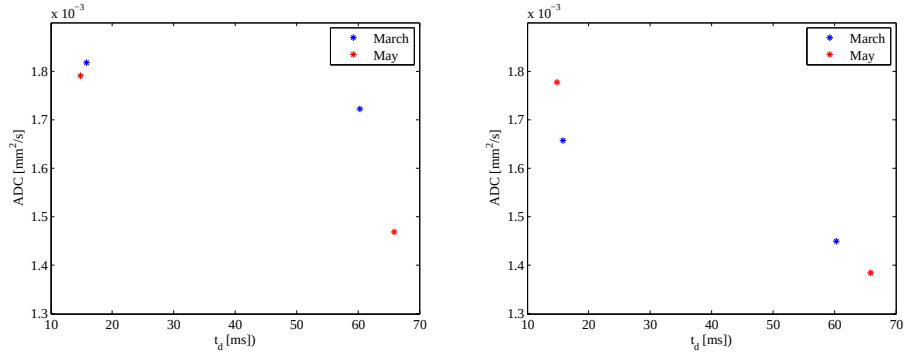

(a) Left breast **(b)** Right breast

Figure 4.3: The measured ADC values of left (4.3a) and right (4.3b) breast for different t_d for volunteer A. The measurements for both sessions are included in the figures. For March: TE = 85 ms. For May TE = 100 ms.

Table 4.1: ADC values registered for subject A for each sequence, Session march, both breast.

Seq. type	TR (ms)	TE (ms)	t_d (ms)	Left breast ADC (mm^2/s)	Right breast ADC (mm^2/s)
MP SE	5300	41	15.8	1.9×10^{-3}	1.4×10^{-3}
MP SE	5300	85	15.8	1.8×10^{-3}	1.7×10^{-3}
MP SE	5300	85	63.5	1.7×10^{-3}	1.4×10^{-3}
MP STEAM	5300	85	196.8	1.0×10^{-3}	0.7×10^{-3}
Sine diff. grad. SE	5300	41	7.1	2.0×10^{-3}	1.9×10^{-3}

Table 4.2: ADC values registered for subject A for each sequence, Session may, both breast.

Seq. type	TR (ms)	TE (ms)	t_d (ms)	Left breast ADC (mm^2/s)	Right breast ADC (mm^2/s)
MP SE	7300	53	14.8	1.5×10^{-3}	1.5×10^{-3}
MP SE	7300	100	14.8	1.8×10^{-3}	1.8×10^{-3}
MP SE	7300	100	65.9	1.5×10^{-3}	1.4×10^{-3}
BP SE	7300	75	8.6	1.9×10^{-3}	2.1×10^{-3}
MP STEAM	7300	54	197.4	1.3×10^{-3}	1.0×10^{-3}
Sine diff. grad. SE	7300	77	7.1	2.1×10^{-3}	2.1×10^{-3}
Cosine diff. grad. SE	7300	111	6.5	1.6×10^{-3}	1.3×10^{-3}

4.2 Volunteer B

4.2.1 T_2 for each b, ADC for each TE, ADC for each t_d

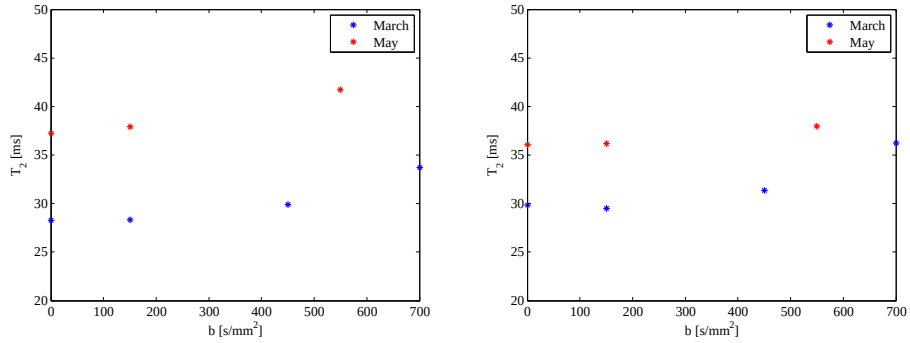

(a) Left breast **(b)** Right breast

Figure 4.4: The measured T_2 values of left (4.4a) and right (4.4b) breast for different b-values for volunteer B. The measurements for both sessions are included in the figures. For March: t_d = 15.8 ms. For May t_d = 14.8 ms.

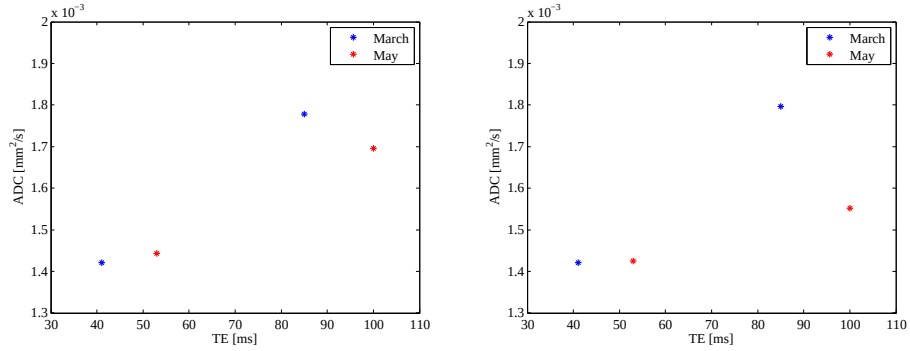

(a) Left breast **(b)** Right breast

Figure 4.5: The measuredADC values of left (4.5a) and right (4.5b) breast for different TE for volunteer B. The measurements for both sessions are included in the figures. For March: t_d = 15.8 ms. For May t_d = 14.8 ms.

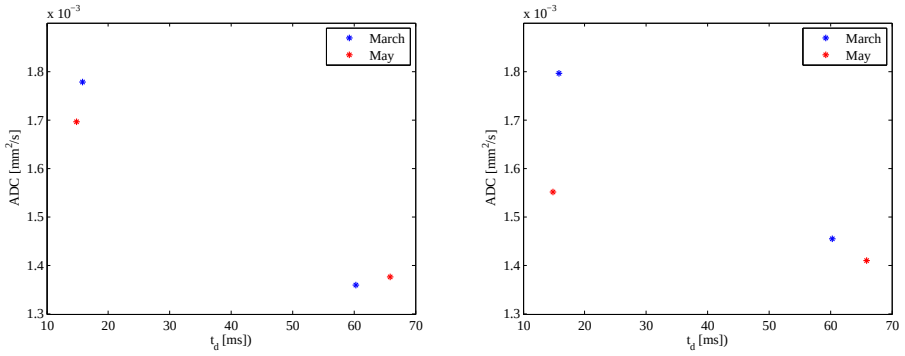

(a) Left breast **(b)** Right breast

Figure 4.6: The measured ADC values of left (4.3a) and right (4.3b) breast for different t_d for volunteer B. The measurements for both sessions are included in the figures. For March: TE = $85\,\mathrm{ms}$. For May TE = $100\,\mathrm{ms}$.

Table 4.3: ADC values registered for subject B, Session march, both breast.

Seq. type	TR (ms)	TE (ms)	t_d (ms)	Left breast ADC (mm^2/s)	Right breast ADC (mm^2/s)
MP SE	5300	41	15.8	1.4×10^{-3}	1.4×10^{-3}
MP SE	5300	85	15.8	1.8×10^{-3}	1.8×10^{-3}
MP SE	5300	85	63.5	1.4×10^{-3}	1.5×10^{-3}
MP STEAM	5300	85	196.8	0.9×10^{-3}	1.4×10^{-3}
Sine diff. grad. SE	5300	41	7.1	1.5×10^{-3}	1.5×10^{-3}

Table 4.4: ADC values registered for subject B for each sequence, Session may, both breast.

Seq. type	TR (ms)	TE (ms)	t_d (ms)	Left breast ADC (mm^2/s)	Right breast ADC (mm^2/s)
MP SE	7300	53	14.8	1.4×10^{-3}	1.4×10^{-3}
MP SE	7300	100	14.8	1.7×10^{-3}	1.6×10^{-3}
MP SE	7300	100	65.9	1.4×10^{-3}	1.4×10^{-3}
BP SE	7300	75	8.6	1.8×10^{-3}	1.7×10^{-3}
MP STEAM	7300	54	197.4	1.0×10^{-3}	1.2×10^{-3}
Sine diff. grad. SE	7300	77	7.1	1.6×10^{-3}	1.6×10^{-3}
Cosine diff. grad. SE	7300	111	6.5	1.3×10^{-3}	1.3×10^{-3}

4.3 Yeast data and model fits

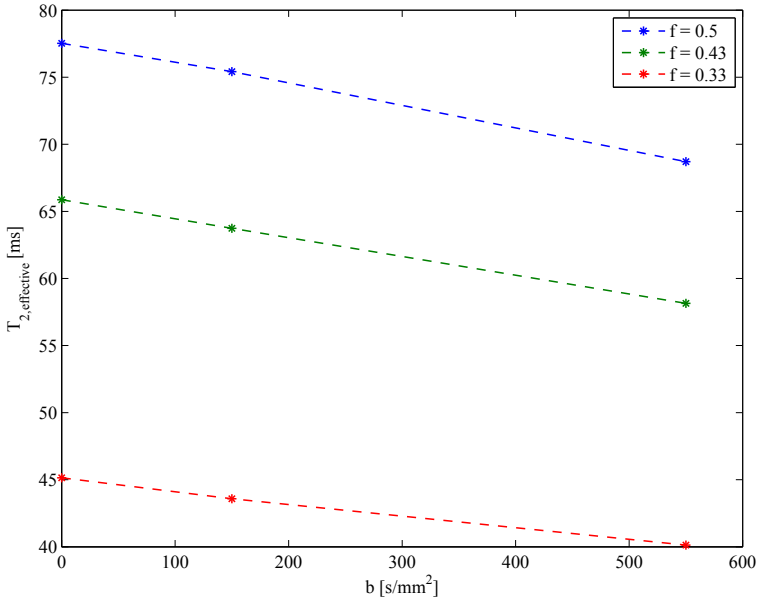

Figure 4.7: The figure presents the estimated values of T_2 as a function of b, for different f

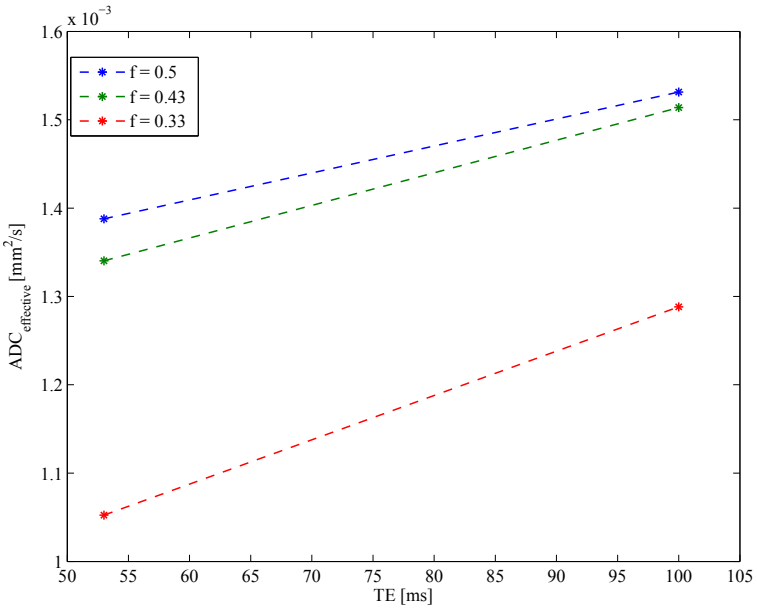

Figure 4.8: ADC is presented as it varies with TE, for different f. Diffusion time t_d is $14.8\,\mathrm{ms}$

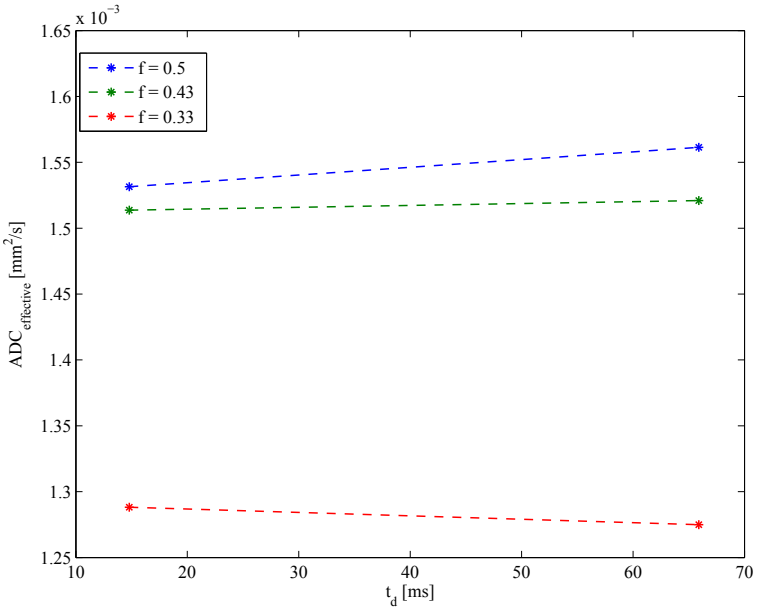

Figure 4.9: In the figure, ADC is shown as it varies with t_d, for different f. Echo time TE = $100\,\mathrm{ms}$

A biexponential fit to the model data yielded a monoexponential function, where $ADC_{\text{slow}} = ADC_{\text{fast}}$ and $T_{2,\text{fast}} = T_{2,\text{slow}}$. This model was subsequently discarded further modeling of the signal.

A monoexponential model is applied to the measured values. The estimated values for S_0 and the effective T_2 and ADC values are presented in tables for each *f*. The fit is made using Equation (2.46).

4.3.1 Monoexponential model fit for $f_{\text{theoretical}} = 0.50$.

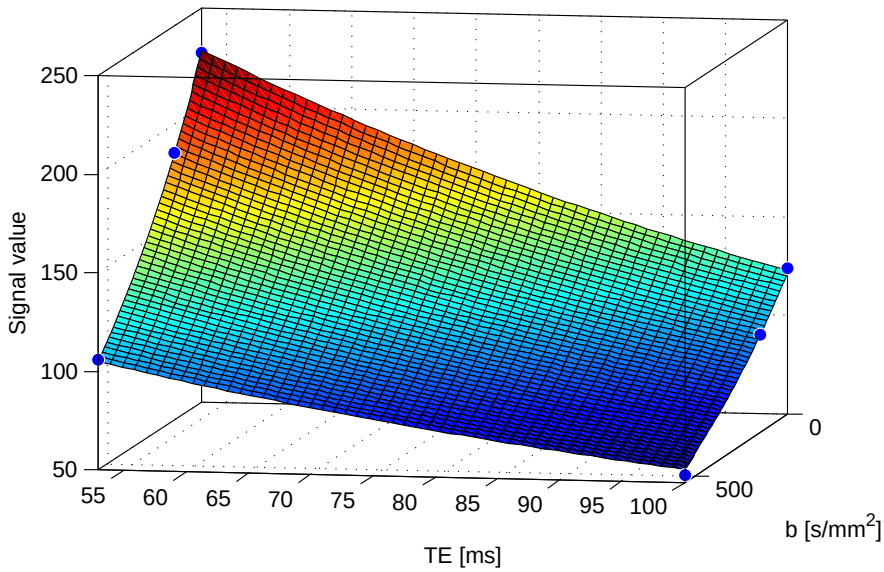

Figure 4.10: The data points collected for the sample prepared with $f_{\text{theoretical}} = 0.50$ is shown as TE and b is varied. A model fit is placed upon the data points.

Table 4.5: The fitting parameters for the biexponential model fit model fit presented in Figure 4.10 are shown below.

S_0	460
$T_{2,\text{effective}}$	$75.7\,\text{ms}$
$ADC_{\text{effective}}$	$1.41 \times 10^{-3}\,\text{mm}^2/\text{s}$

4.3.2 Monoexponential model fit for $f_{\text{theoretical}} = 0.43$.

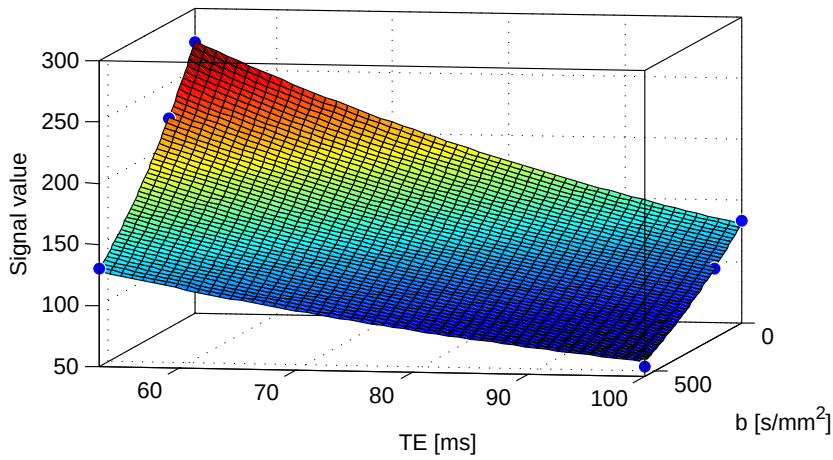

Figure 4.11: The data points collected for the sample prepared with $f_{\text{theoretical}} = 0.43$ is shown as TE and b is varied. A model fit is placed upon the data points.

Table 4.6: The fitting parameters for the biexponential model fit model fit presented in Figure 4.11 are shown below.

S_0	623
$T_{2,\text{effective}}$	$64.1\,\text{ms}$
$ADC_{\text{effective}}$	$1.37 \times 10^{-3}\,\text{mm}^2/\text{s}$

4.3.3 Monoexponential model fit for $f_{\text{theoretical}} = 0.33$.

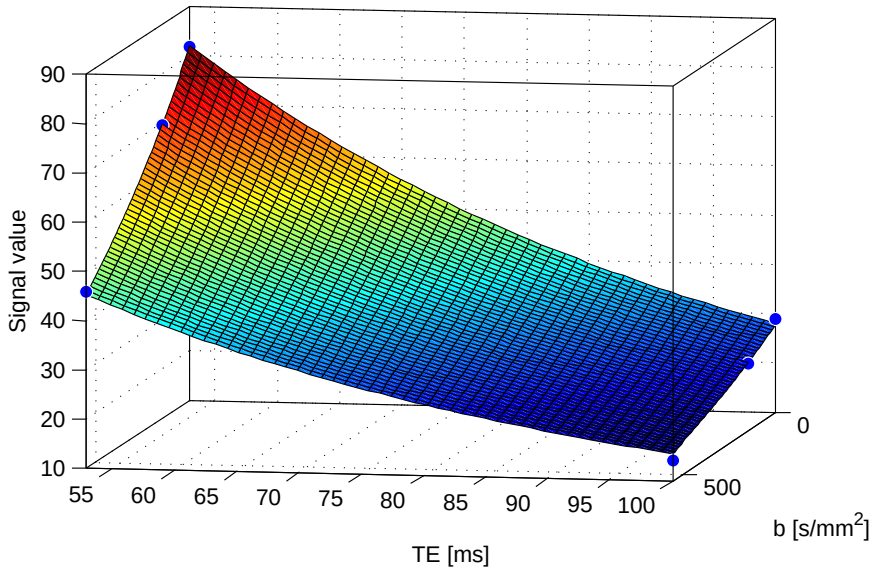

Figure 4.12: The data points collected for the sample prepared with $f_{\text{theoretical}} = 0.33$ is shown as TE and b is varied. A model fit is placed upon the data points.

Table 4.7: The fitting parameters for the biexponential model fit model fit presented in Figure 4.12 are shown below.

S_0	275
$T_{2,\text{effective}}$	$43.8\,\text{ms}$
$ADC_{\text{effective}}$	$1.08 \times 10^{-3}\,\text{mm}^2/\text{s}$

4.3.4 Analysis of monoexponential data

The fitting parameters obtained in the section above is summarized in Table 4.8.

Table 4.8: Monoexponential fitting of parameters

	f = 0.50	f = 0.43	f = 0.33
$T_{2,\text{effective}}$ (ms)	75.7	64.1	43.8
$ADC_{\text{effective}}$ (mm^2/s)	1.41×10^{-3}	1.37×10^{-3}	1.08×10^{-3}

The values in Table 4.8 were plotted and presented in Figure 4.13 and Figure 4.14, together with model fits.

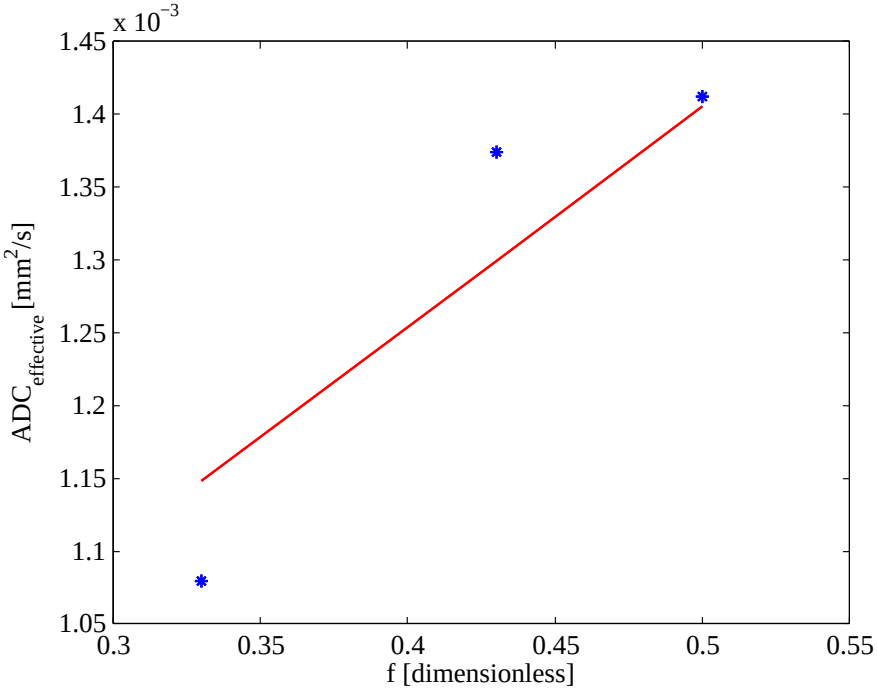

Figure 4.13: The effective ADC was plotted together with a model: $ADC = f \cdot D_{\text{fast}} + (1-f) \cdot D_{\text{slow}}$. The value for D_{fast} was set to be equal to the diffusion constant for water at room temperature, $2.162 \times 10^{-3}\,\text{mm}^2/\text{s}$. The value for D_{slow} from the fit was $6.49 \times 10^{-4}\,\text{mm}^2/\text{s}$.

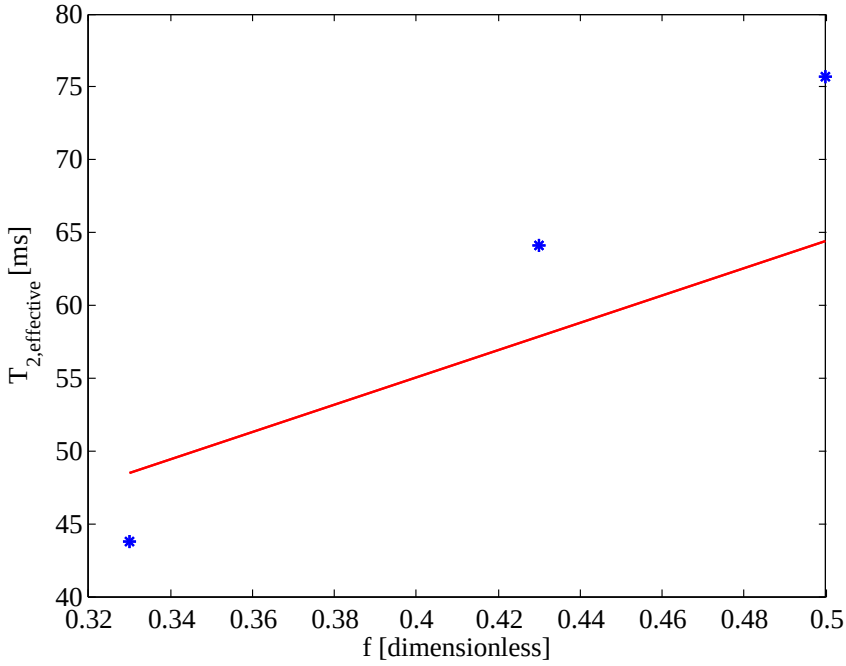

Figure 4.14: The effective T_2 was plotted together with a model: $T_2 = (f/T_{2,\text{fast}} + (1-f)/T_{2,\text{slow}})^{-1}$. The value for $T_{2,\text{fast}}$ was set to be equal to the T_2 for water, 2000 ms. The value for $T_{2,\text{slow}}$ from the fit was 32.7 ms.

Chapter 5

Discussion

5.1 Model selection

The biexponential model failed in fitting the yeast data obtained. The range of b values was not very large, thereby prohibiting the appearance of the slow diffusing compartment. The biexponential fit produced in essence a monoexponential fit, where $ADC_{\text{slow}} = ADC_{\text{fast}}$ and $T_{2,\text{fast}} = T_{2,\text{slow}}$. The further use of a biexponential fitting function was on the basis of this discarded. The use of the slow exchange monoexponential model given in Equation (2.46), with results presented in Figure 4.14 and 4.13, provided an estimate for the ADC and T_2 of the slowly diffusing pool, which is assumed to be the signal arising from the yeast cells. It did not provide a very good fit, as is evidenced by the behaviour of the model in Figure 4.14.

5.2 Choice of *f*

The free volume fraction f was calculated from the amount of water added to the fresh yeast. As an example a packet of $50\,\mathrm{g}$ fresh yeast mixed with $50\,\mathrm{g}$ of water makes for $f = 1/2$. The rigid assumption in specifying f may not be valid. The residual water fraction of a packet of fresh yeast is by one source approximated to be $1/6$ [22]. Another assumption is that the yeast when suspended will not conflate or expand, and thereby shifting the true f, leading to a overestimation of the experimental f. A way approximate the value of f is to perform a microscopy session with the prepared solution. By way of counting the cells in present in the image, the cellularity could have been determined.

5.3 Exploration of degrees of freedom

The analysis of yeast suspensions as a function of water fraction, b-value, echo time and diffusion time were inhibited by limited experimental values. The choice of three f's and b's, and two diffusion and echo times made for difficulty in elucidating the properties of

the system investigated. It is also worth mentioning that the measurements at b-values higher than $700\,\mathrm{s/mm^2}$ from the first session with volunteers were discarded due to very low signal to noise values.

5.4 Comparing across diffusion sequences

The difficulty in fixing all but one variable and observing the change in signal across all diffusion sequences was difficult. The ability to prepare and tune sequences when the MR scanner was not without complication. The change in one variable could force the change in another, thus limiting the ability to control which variable to explore.

5.5 Breast tissue

Fat suppression was performed in the sequences applied. It is from this assumed that the signal obtained would originate only from fibroglandular tissue. This may not be the case for larger b-values, where the slow diffusion of fat will contribute to the signal aquired. The suppression of fat signal is not absolute, and at higher b values there may be the case that no signal remains except the signal originating from fat. In this experiment, where the b-values used is mild, the presence of fat is assumed to not be of great influence.

5.6 Fitting biophysical models to *in vivo* data

Difficulties were apparent when attempting to fit models to the data provided by the volunteers. There is large variation present in the estimated parameters comparing left and right breast and subjects. It may be of more interest to discuss the trends in the parameters obtained. It can be observed that there is a reduction in ADC value based on diffusion time for both subjects and both breasts. This can be an indication of a level of restriction apparent separating the two diffusion times. It is difficult to discuss the meaning of this depression in ADC value, when the ADC value calculated is the directionally averaged ADC. Biological tissue is highly anistropic, but some tissue have symmetry which can be detected by diffusion tensor imaging. This was unfortunately outside of the scope of the work done.

5.7 Phase direction bias

Eddy current distortions of the images were detected. The resulting distortions can be observed by noting the difference between Figure 5.1a and 5.1b. Choosing an ROI to use for further analysis will be influenced on what image to use, and where in the tissue the ROI is placed.

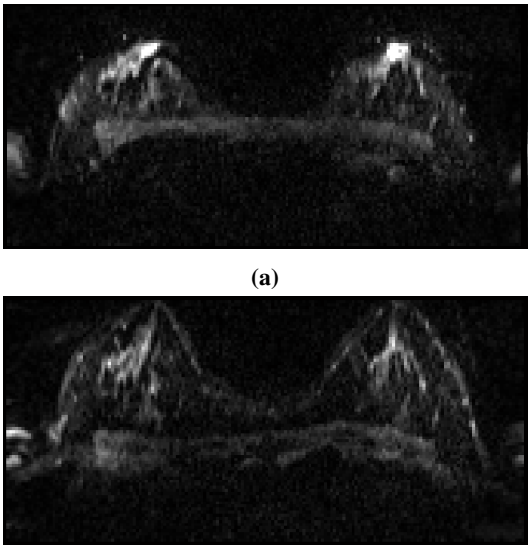

(a)

(b)

Figure 5.1: Significant eddy current image distortion was detected in the images taken. Both images are from the same slice. In 5.1a, the phase direction follows a anterior to posterior directionality. The opposite for 5.1b, phase direction from posterior to anterior.

5.8 Signal from yest cells

Diffusing water molecules can in a time t_d have the possibility to have diffused for a length $d = \sqrt{6D_0t_d}$, by manipulating Equation (2.34). For a t_d of $14\,\mathrm{ms}$ and a D_0 of $1 \times 10^{-3}\,\mathrm{mm}^2/\mathrm{s}$, the value of d will be $13\,\mu\mathrm{m}$. For a cell size of $4\,\mu\mathrm{m}$, there is a high probability of signal loss due to spins ending up at virtually the same location at the application of the secondary diffusing pulse.

The yeast cells in suspension was approximated to be stationary throughout the experiment. The averages calulated was based on directionally averaging, with the assumption that no direction is favored when calculating diffusion. As was observed in the solutions prepared, some sedimentation was present after the conclusion of the experiment. This would have the effect of skewing the value of f based when the samples were subjected to each sequence.

The diffusion of cells are assumed to be neglible for the results obtained. Using the Stokes-Einstein relation for calculating the diffusion coefficient of cells gives $D = \frac{k_b \cdot T}{6\pi\eta r} \approx 5 \times 10^{-8}\,\mathrm{mm}^2/\mathrm{s}$. Based on this, the impact of cells transporting its comprising spins and thereby affecting the resulting diffusion signal is not taken into account. But, the motion of cells due to gravity could have had an effect on the measurements.

Chapter 6

Conclusion

Novel MR scanner software was used to measure the MR signal in fibroglandular breast tissue *in vivo*, and in prepared solutions of Bakers Yeast. The ADC values and T_2 values were calculated in both systems. An attemt to model the signal behaviour in yeast was made. Across the range of b values explored, T_2 varied. Likewise, the value of ADC varied across the echo times studied. This suggest some dependence of T_2 on b and of ADC on echo time. Changes in ADC value was detected when only varying the experimental diffusion time.

Bibliography

[1] OECD/EU. Health at a glance: Europe 2016. 2016. URL http://dx.doi.org/10.1787/9789264265592-en.

[2] gov.uk. Mri procedures: protection of patients and volunteers. 2016. URL https://www.gov.uk/government/uploads/system/uploads/attachment_data/file/329364/Protection_of_patients_and_volunteers_undergoing_MRI_procedures.pdf.

[3] Maggie A Flower. Webb's physics of medical imaging. CRC Press, 2012.

[4] John Lilley. Nuclear physics: principles and applications. John Wiley & Sons, 2013.

[5] Derek K Jones. Diffusion mri. Oxford University Press, 2010.

[6] E Mark Haacke, Robert W Brown, Michael R Thompson, Ramesh Venkatesan, et al. Magnetic resonance imaging: physical principles and sequence design, volume 82. Wiley-Liss New York:, 2014.

[7] Jens O. Andersen. Introduction to statistical mechanics. Akademika forlag, 2012.

[8] Edward O Stejskal and John E Tanner. Spin diffusion measurements: spin echoes in the presence of a time-dependent field gradient. The journal of chemical physics, 42 (1):288–292, 1965.

[9] Jens Frahm, Klaus-Dietmar Merboldt, and Wolfgang Hänicke. Localized proton spectroscopy using stimulated echoes. Journal of Magnetic Resonance (1969), 72(3): 502–508, 1987.

[10] B Gross and R Kosfeld. Anwendung der spin-echo-methode der messung der selbstdiffusion. Messtechnik, 77:171–177, 1969.

[11] Andrew L Alexander, Jay S Tsuruda, and Dennis L Parker. Elimination of eddy current artifacts in diffusion-weighted echo-planar images: the use of bipolar gradients. Magnetic Resonance in Medicine, 38(6):1016–1021, 1997.

[12] Eitzik Smouha and Michal Neeman. Compartmentation of intracellular water in multicellular tumor spheroids: diffusion and relaxation nmr. Magnetic resonance in medicine, 46(1):68–77, 2001.

[13] Horst Feldmann. Yeast: molecular and cell biology. John Wiley & Sons, 2011.

[14] photo by Bob Blaylock Wikipedia. Baker's yeast — wikipedia, the free encyclopedia, 2017. URL https://en.wikipedia.org/w/index.php?title=Baker%27s_yeast&oldid=782625068. [Online; accessed 24-June-2017].

[15] Richard Drake, A Wayne Vogl, and Adam WM Mitchell. Gray's Anatomy for Students E-Book. Elsevier Health Sciences, 2009.

[16] Emmanuelle M Delfaut, Javier Beltran, Glyn Johnson, Jean Rousseau, Xavier Marchandise, and Anne Cotten. Fat suppression in mr imaging: techniques and pitfalls. Radiographics, 19(2):373–382, 1999.

[17] medical illustrator Patrick J. Lynch. Breast anatomy normal, 2006. URL https://commons.wikimedia.org/wiki/File:Breast_anatomy_normal.jpg#. [Online; accessed 24-June-2017].

[18] SIEMENS. Siemens 3 t magnetom prisma technical details, 2016. https://www.healthcare.siemens.com/magnetic-resonance-imaging/3t-mri-scanner/magnetom-prisma/technical-details [Accessed: 2016-12-14].

[19] Mathworks inc. South Natick MA.

[20] William D Penny, Karl J Friston, John T Ashburner, Stefan J Kiebel, and Thomas E Nichols. Statistical parametric mapping: the analysis of functional brain images. Academic press, 2011.

[21] NTNU Pål Erik Goa, Associate professor. Mripsto2.

[22] JE Tanner. Intracellular diffusion of water. Archives of Biochemistry and Biophysics, 224(2):416–428, 1983.

Appendix

6.1 Yeast measurements, April 28 2017.

Table 6.1: Signal intensities for each yeast mixing fraction each experimental b-value. Monopolar diffusion gradient. *TR* = 5300 ms, *TE* = 53 ms, t_d = 14.8 ms.

	Signal intensity		
b (s/mm^2)	f = 0.5	f = 0.43	f = 0.33
0	123.9023	271.9429	81.8140
150	99.6006	221.7505	69.5094
550	53.5277	130.0091	45.7999

Table 6.2: Signal intensities for each yeast mixing fraction each experimental b-value. Monopolar diffusion gradient. *TR* = 6800 ms, *TE* = 100 ms, t_d = 14.8 ms.

	Signal intensity		
b (s/mm^2)	f = 0.5	f = 0.43	f = 0.33
	0 123.9023	133.2217	28.8837
150	99.6006	106.0799	23.6447
550	53.5277	57.9324	14.1959

Table 6.3: Signal intensities for each yeast mixing fraction each experimental b-value. Monopolar diffusion gradient. *TR* = 6800 ms, *TE* = 100 ms, t_d = 68.7 ms.

	Signal intensity		
b (s/mm^2)	f = 0.5	f = 0.43	f = 0.33
0	123.8542	133.4872	28.5031
150	99.0102	106.1804	23.5955
550	52.6185	57.8167	14.1456

Table 6.4: Signal intensities for each yeast mixing fraction each experimental b-value. Oscilating (Cosine) diffusion gradient. TR = 7300 ms, TE = 111 ms, t_d = 6.5 ms.

	Signal intensity		
b (s/mm^2)	f = 0.5	f = 0.43	f = 0.33
0	109.2814	111.6611	23.3083
150	85.4301	87.6102	18.8560
550	44.3400	46.3507	11.1298

Table 6.5: Signal intensities for each yeast mixing fraction each experimental b-value. Oscilating (Sine) diffusion gradient. TR = 5800 ms, TE = 77 ms, t_d = 7.1 ms.

	Signal intensity		
b (s/mm^2)	f = 0.5	f = 0.43	f = 0.33
0	165.8164	182.5923	48.2176
150	130.1668	144.3033	39.8017
550	69.6264	78.9935	24.7790

Table 6.6: Signal intensities for each yeast mixing fraction each experimental b-value. Bipolar diffusion gradient. TR = 5700 ms, TE = 75 ms, t_d = 8.6 ms.

	Signal intensity		
b (s/mm^2)	f = 0.5	f = 0.43	f = 0.33
0	158.7320	182.0812	39.4421
150	125.8280	144.2299	32.3169
550	68.4991	80.4687	20.2933

Table 6.7: Signal intensities for each yeast mixing fraction each experimental b-value. STEAM diffusion sequence. TR = 5700 ms, TE = 63 ms, t_d = 197.4 ms, T_{mix} = 177 ms.

	Signal intensity	
b (s/mm^2)	f = 0.5	f = 0.43
0	117.8294	74.7241
150	101.8367	62.7215
550	56.3664	36.1359

6.2 Volunteer scan I, March 21 2017.

6.2.1 Scan of volunteer A, March 21 2017.

Table 6.8: Signal intensities for breast tissue of volunteer A. Monopolar diffusion sequence. *TR* = 5300 ms, *TE* = 41 ms, t_d = 15.8 ms.

	Signal intensity	
b (s/mm^2)	Left breast	Right breast
0	87.4278	70.9741
150	63.1527	50.0495
450	35.0955	32.3750
700	4.6645	21.5087
1200	12.1767	12.2426

Table 6.9: Signal intensities for breast tissue of volunteer A. Monopolar diffusion sequence. *TR* = 5300 ms, *TE* = 85 ms, t_d = 15.8 ms.

	Signal intensity	
b (s/mm^2)	Left breast	Right breast
0	27.0371	19.4414
150	20.2092	13.8347
450	11.2467	8.2758
700	7.4091	7.3683
1200	5.3471	5.9253

Table 6.10: Signal intensities for breast tissue of volunteer A. Monopolar diffusion sequence. TR = 5300 ms, TE = 85 ms, t_d = 60.3 ms.

	Signal intensity	
b (s/mm^2)	Left breast	Right breast
0	26.9604	17.0655
150	19.5869	12.9566
450	11.3056	7.9985
700	8.0979	6.2373
1200	5.7150	4.7647
1800	5.2718	4.5522
2400	4.9698	4.2681
3000	4.9350	4.3203

Table 6.11: Signal intensities for breast tissue of volunteer A. Oscilating (sine) diffusion sequence. TR = 6100 ms, TE = 85 ms, t_d = 7.1 ms.

	Signal intensity	
b (s/mm^2)	Left breast	Right breast
0	30.6906	19.5655
150	21.6852	14.0407
450	11.5199	7.9955
700	7.6787	6.0216

Table 6.12: Signal intensities for breast tissue of volunteer A. STEAM diffusion sequence. TR = 5300 ms, TE = 85 ms, t_d = 196.8 ms, T_{mix} = 136.5 ms.

	Signal intensity	
b (s/mm^2)	Left breast	Right breast
0	7.6371	5.0358
150	6.2027	4.2141
450	4.3776	3.3182
700	3.7198	3.1579
1200	3.1810	3.0312
1800	3.0322	2.8703
2400	2.9568	2.9336
3000	2.9177	2.9143

6.2.2 Scan of volunteer B, March 21 2017.

Table 6.13: Signal intensities for breast tissue of volunteer B. Monopolar diffusion sequence. *TR* = 5300 ms, *TE* = 41 ms, t_d = 15.8 ms.

	Signal intensity	
b (s/mm^2)	Left breast	Right breast
0	69.4531	64.7217
150	51.4114	48.2092
450	30.3010	28.5618
700	19.8870	18.2552
1200	11.9801	10.0967

Table 6.14: Signal intensities for breast tissue of volunteer B. Monopolar diffusion sequence. *TR* = 5300 ms, *TE* = 85 ms, t_d = 15.8 ms.

	Signal intensity	
b (s/mm^2)	Left breast	Right breast
0	14.6328	14.8113
150	10.8658	10.8397
450	6.9602	7.0194
700	5.3878	5.4186
1200	4.3907	4.2937

Table 6.15: Signal intensities for breast tissue of volunteer B. Monopolar diffusion sequence. TR = 5300 ms, TE = 85 ms, t_d = 60.3 ms.

	Signal intensity	
b (s/mm^2)	Left breast	Right breast
0	14.5703	14.7406
150	10.0333	10.6168
450	6.9221	6.8049
700	5.4320	5.2606
1200	4.2909	4.2853
1800	3.8543	4.1712
2400	3.8395	4.1435
3000	3.8501	3.8852

Table 6.16: Signal intensities for breast tissue of volunteer B. Oscilating (sine) diffusion sequence. TR = 6100 ms, TE = 85 ms, t_d = 7.1 ms.

	Signal intensity	
b (s/mm^2)	Left breast	Right breast
0	18.5234	16.6557
150	13.7371	12.4608
450	8.1699	7.6331
700	6.3256	5.8448

Table 6.17: Signal intensities for breast tissue of volunteer B. STEAM diffusion sequence. TR = 5300 ms, TE = 85 ms, t_d = 196.8 ms, T_{mix} = 136.5 ms.

	Signal intensity	
b (s/mm^2)	Left breast	Right breast
0	6.1049	9.5467
150	5.5136	7.1491
450	4.0417	4.6223
700	3.3475	3.7018
1200	3.1071	3.1260
1800	2.9601	2.9003
2400	2.9773	2.7844
3000	2.9888	2.8315

6.3 Volunteer scan II, May 9 2017.

6.3.1 Scan of volunteer A, May 9 2017.

Table 6.18: Signal intensities for breast tissue of volunteer A. Monopolar diffusion sequence. *TR* = 7300 ms, *TE* = 53 ms, t_d = 14.8 ms.

	Signal intensity	
b (s/mm^2)	Left breast	Right breast
0	70.1381	55.5684
150	52.9563	42.2173
550	26.1138	20.8629

Table 6.19: Signal intensities for breast tissue of volunteer A. Monopolar diffusion sequence. *TR* = 7300 ms, *TE* = 100 ms, t_d = 14.8 ms.

	Signal intensity	
b (s/mm^2)	Left breast	Right breast
0	20.1152	14.7740
150	15.5671	10.9998
550	8.6200	6.3552

Table 6.20: Signal intensities for breast tissue of volunteer A. Monopolar diffusion sequence. *TR* = 7300 ms, *TE* = 100 ms, t_d = 65.9 ms.

	Signal intensity	
b (s/mm^2)	Left breast	Right breast
0	19.5723	14.3441
150	14.7997	11.3539
550	8.5926	6.6509

6.3.2 Scan of volunteer B, May 9 2017.

Table 6.21: Signal intensities for breast tissue of volunteer A. Bipolar diffusion sequence. *TR* = 7300 ms, *TE* = 75 ms, t_d = 8.6 ms.

	Signal intensity	
b (s/mm^2)	Left breast	Right breast
0	45.7170	34.6470
150	33.9514	25.4659
550	15.8908	11.1003

Table 6.22: Signal intensities for breast tissue of volunteer A. STEAM with monopolar diffusion sequence. *TR* = 7300 ms, *TE* = 54 ms, t_d = 197.4 ms, T_{mix} = 177 ms.

	Signal intensity	
b (s/mm^2)	Left breast	Right breast
0	25.5552	15.2635
150	21.7027	13.2138
550	12.5666	8.6036

Table 6.23: Signal intensities for breast tissue of volunteer A. Oscillating (sine) diffusion sequence. *TR* = 7300 ms, *TE* = 77 ms, t_d = 7.1 ms.

	Signal intensity	
b (s/mm^2)	Left breast	Right breast
0	32.4333	22.6297
150	22.5028	15.8865
550	9.9955	7.1765

Table 6.24: Signal intensities for breast tissue of volunteer A. Oscillating (cosine) diffusion sequence. *TR* = 7300 ms, *TE* = 111 ms, t_d = 6.5 ms.

	Signal intensity	
b (s/mm^2)	Left breast	Right breast
0	13.2674	8.3095
150	9.6224	6.3275
550	5.4650	3.9080

Table 6.25: Signal intensities for breast tissue of volunteer B. Monopolar diffusion sequence. *TR* = 7300 ms, *TE* = 53 ms, t_d = 14.8 ms.

	Signal intensity	
b (s/mm^2)	Left breast	Right breast
0	74.1685	65.7516
150	55.3205	51.1248
550	28.8840	27.8749

Table 6.26: Signal intensities for breast tissue of volunteer B. Monopolar diffusion sequence. *TR* = 7300 ms, *TE* = 100 ms, t_d = 14.8 ms.

	Signal intensity	
b (s/mm^2)	Left breast	Right breast
0	21.0091	17.8702
150	16.0042	13.9344
550	9.3603	8.0858

Table 6.27: Signal intensities for breast tissue of volunteer B. Monopolar diffusion sequence. *TR* = 7300 ms, *TE* = 100 ms, t_d = 65.9 ms.

	Signal intensity	
b (s/mm^2)	Left breast	Right breast
0	21.6680	18.5768
150	16.6767	14.3996
550	10.0132	8.4565

Table 6.28: Signal intensities for breast tissue of volunteer B. Bipolar diffusion sequence. TR = 7300 ms, TE = 75 ms, t_d = 8.6 ms.

	Signal intensity	
b (s/mm^2)	Left breast	Right breast
0	36.5682	31.7813
150	26.6694	23.6674
550	13.5690	12.0552

Table 6.29: Signal intensities for breast tissue of volunteer B. STEAM with monopolar diffusion sequence. TR = 7300 ms, TE = 54 ms, t_d = 197.4 ms, T_{mix} = 177 ms.

	Signal intensity	
b (s/mm^2)	Left breast	Right breast
0	22.4203	26.6860
150	19.2061	22.3590
550	12.8046	13.4762

Table 6.30: Signal intensities for breast tissue of volunteer B. Oscillating (sine) diffusion sequence. TR = 7300 ms, TE = 77 ms, t_d = 7.1 ms.

	Signal intensity	
b (s/mm^2)	Left breast	Right breast
0	20.7240	22.5819
150	15.4569	17.1708
550	8.3438	9.3235

Table 6.31: Signal intensities for breast tissue of volunteer B. Oscillating (cosine) diffusion sequence. TR = 7300 ms, TE = 111 ms, t_d = 6.5 ms.

	Signal intensity	
b (s/mm^2)	Left breast	Right breast
0	7.0971	8.5413
150	5.5247	6.6808
550	3.4162	4.0213